Nematic Ordering of Polymers in Confined Geometry Applied to DNA Packaging in Viral Capsids

ARTICLE *in* THE JOURNAL OF PHYSICAL CHEMISTRY B · JANUARY 2011

Impact Factor: 3.3 · DOI: 10.1021/jp108461z · Source: PubMed

4 AUTHORS, INCLUDING:

Nikolay Oskolkov
Lund University
14 PUBLICATIONS **90** CITATIONS

SEE PROFILE

Nematic Ordering of Polymers in Confined Geometry Applied to DNA Packaging in Viral Capsids

Nikolay N. Oskolkov,*,† Per Linse,‡ Igor I. Potemkin,§ and Alexei R. Khokhlov§

Department of Chemistry, University of North Carolina, Chapel Hill, North Carolina 27599-3290, United States; Division of Physical Chemistry, Department of Chemistry, Lund University, S-221 00 Lund, Sweden; and Physics Department, Moscow State University, 119992 Moscow, Russia

Received: September 5, 2010; Revised Manuscript Received: November 5, 2010

A density functional theory of the spatial distribution and biaxial nematic order of polymers of arbitrary length and rigidity inside a spherical cavity is proposed. The local order of different chain segments is considered as an alignment to a spatially varying director field of cylindrical symmetry. The steric interactions are taken into account in the second virial approximation. Polymer density and orientational order distributions inside the spherically cavity are the principal results. It was found that short and flexible polymers were located at the center of the sphere and were orientationaly disordered. Upon increasing polymer length and/or polymer rigidity, the location of the polymer was continuously shifted toward the surface of the spherical cavity and the polymer segments became gradually more aligned. Parameters have been selected to model the behavior of genomes in spherical viral capsids.

1. Introduction

The behavior of confined polymers is very different from that of free polymers, and sometimes difficult to understand intuitively. For instance, it is known[1] that an ideal polymer chain of length N squeezed into a cylindrical pore (tube) is not affected by the confinement along the contour of the tube, i.e., its size along the tube $R \approx aN^{1/2}$, where a is the size of the monomeric unit. This is an important consequence of the description of the ideal chain as a random walk that is independent along each coordinate, so the deformation of the ideal chain in one direction does not affect its behavior in other directions. On the other hand, a chain with excluded volume interactions being localized in the tube is stretched along the contour of the tube, $R \sim aN$. The physical reason for this stretching is the penalty due to overlapping of the segments of the chain with excluded volume interactions, which was absent for the case of ideal chain. Furthermore, the size of an ideal polymer chain confined to a spherical pore of the size $D < aN^{1/2}$ is determined only by the size of the pore, $R \sim D$ and does not depend at all on the length N of the chain. All these examples demonstrate that confined polymers are quite difficult to physically understand even on the simplest level of ideal chains. Biological polymers usually have additional degrees of freedom such as excluded volume interactions, rigidity, and charge that provides a huge variety of effects in confined geometries. One of the interesting examples of biological polymers in confined geometry appears in viruses.

Viruses are unique objects which represent Nature's simplest biological system that at the same time is relatively easy to study.[2] Viruses consist of two main components: a viral capsid that is a hollow container made by polypeptides and a genome that can be a double-/single-stranded DNA/RNA. The viruses containing double-stranded DNA are usually formed through initial formation of a capsid with the following loading of the genome by a molecular motor mechanism. In contrast, the viruses with single-stranded DNA/RNA are created in the presence of genome by self-assembly of the genetic material with components of the capsid (capsomers). The persistence length of a double-stranded DNA is typically of the same order of magnitude as the size of the capsid (≈50 nm), and the elastic bending energy plays a dominant role in the process of packaging and ejection of the genome. This is also the reason why the pressure inside the capsid with double-stranded DNA can be very high (≈50 atm).[3] On the other hand, a single-stranded genome is relatively flexible, and its persistence length (well-defined for linear parts of the genome) is only a few nanometers, which is much smaller than the size of capsid.

The packaging of genomes in viruses has been studied for many years both experimentally[3−8] and theoretically.[9−38] Historically, theoretical studies regarding viral capsids evolved in two directions. The first direction was focused on genome encapsidation through self-assembly of the genome and capsomers,[10−12] which is typical for flexible single-stranded RNA. Here, we are mostly interested in the second direction, which is aimed at understanding the packaging of double-stranded DNA[13−17] as well as the conformation of stiff double-stranded genome inside viral capsids of different geometries.[18−32] For the simplest case of capsids with spherical or icosahedral symmetry, the most common reported structures of double-stranded DNA were spool,[13,14,16,28] helix,[19] torus,[13,14] and folded torus.[31,32] In most of the theoretical works,[13−15,17,25,26] the conformation of the packaged genome was assumed to be known a priori. The parameters of the system were calculated for a certain packaging scenario by minimization of the free energy containing contributions from elastic bending energy as well as steric and electrostatic interactions.

More general approaches that are not based on a predefined genome structure have been recently used to study conforma-

* To whom correspondence should be addressed. E-mail: oskolkov@polly.phys.msu.ru.
† University of North Carolina.
‡ Lund University.
§ Moscow State University.

10.1021/jp108461z
Published on Web 12/27/2010

tions and structural transitions of a polymer in confined geometry.[18,20−24] A disordered−ordered (spiral) state transition at increasing persistence length of the chain strictly confined onto a spherical surface was found by Monte Carlo simulations and scaling analysis.[18,20] A statistical theory based on the Edwards approach studying the conformation of an elastic rod packed onto a spherical surface shows that the confinement induces a configurational phase transition from a disordered (isotropic) phase to an ordered (nematic) phase.[21,22] An inverse spool packaging scenario was found using the director-field model.[23,24]

Here, we develop a density functional theory[25] describing the behavior of a single polymer of arbitrary length and flexibility confined inside a sphere. The theory is based on a method proposed by Onsager[39−41] for rigid polymers in bulk solution but applied to a spherically confined polymer, where the confinement imposes steric constraints on the polymer. The interaction between polymer segments is described using a second viral expression. Our theory provides the density and order distributions of the polymer in the confining sphere as a function of polymer contour length, polymer persistence length, polymer diameter, and the size of the confining sphere. In particular, we demonstrate that increased (nematic) order is obtained by increasing the contour length and/or persistence length of the polymer. We apply the approach using parameters representative of various genomes inside spherical capsids. In particular, we illustrate two limiting packaging cases: (i) the short and moderately stiff genome is localized preferentially at the center of the capsid and is orientationally disordered and (ii) the long and stiff genome is preferentially located closer to the capsid surface and displays a nematic order. The origin of the nematic order and its biaxiality imposed by the surface of the sphere as well as the physical reasons of the polymer displacement toward the surface while stiffening are discussed.

2. Model and Method

In bulk, a disordered solution of long and rigid macromolecules (rods) undergoes a nematic transition upon increasing rod concentration.[39] The rod turns out to be preferentially aligned along a direction (referred to as a director) that is *constant* throughout the bulk. The same disorder−order state transition was shown to appear for macromolecules with freely jointed and wormlike mechanisms of rigidity.[40,41] An investigation of semiflexible macromolecules in a confined geometry is a more complicated problem. Due to the constraints imposed by the surface of the sphere, the nematic order occurs with, generally, a spatially *varying* director.

Specifically, let us consider a sphere of radius R containing a semiflexible polymer of contour length L, persistence length l_p, and cross-section diameter d (Figure 1). Consider a small volume element inside the sphere at the point $\mathbf{r}$. Denote unit vectors connecting bonded segments generally by $\mathbf{n}(\mathbf{r})$. The tendency of alignment of nearby unit vectors increases as the segment concentration in the volume element is increased. Moreover, denote the averaged direction in the volume element by $\mathbf{u}(\mathbf{r})$, which hence is a local director at $\mathbf{r}$. The director $\mathbf{u}(\mathbf{r})$ is generally different in various volume elements; hence, $\mathbf{u}(\mathbf{r})$ is a vector field. The a priori determination of the director field from elastic continuum theory[42,43] is generally a complicated talk. To simplify, we here postulate that director field rotates around, say the Z axis of the sphere, with its direction in the XY plane being perpendicular to $\mathbf{r}$. Thus, we impose that the director field has cylindrical symmetry.[27] We argue that this is a reasonable simplification since it is able to describe the most important aspects genome structures such as spoollike and torus conformations.[5]

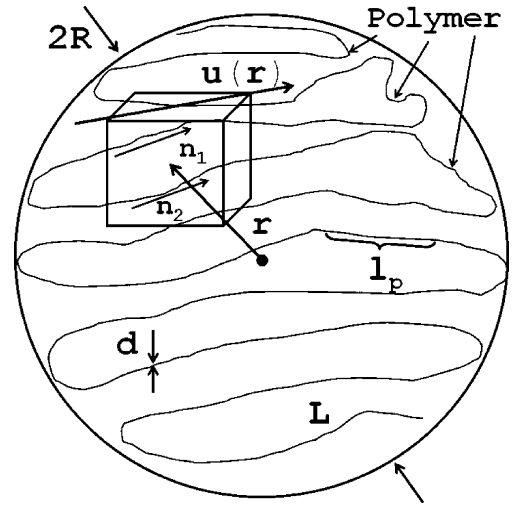

Figure 1. Schematic picture illustrating the nematic order of a semiflexible polymer confined inside a sphere. Here, $\mathbf{u}(\mathbf{r})$ is local director of the volume element at $\mathbf{r}$, and $\mathbf{n}_1(\mathbf{r})$ and $\mathbf{n}_2(\mathbf{r})$ are unit vectors connected with two segments of the chain located in the volume element.

Let us introduce the generalized density $\rho(\mathbf{n},\mathbf{r})$ that depends on both spatial $\mathbf{r} = (r,\Theta,\Phi)$ and orientational $\mathbf{n} = (\theta,\phi)$ coordinates. The generalized density can be expressed in a standard way as a product of wave functions[44,45] according to

$$\rho(\mathbf{n},\mathbf{r}) = \psi(-\mathbf{n},\mathbf{r})\psi(\mathbf{n},\mathbf{r}) \tag{1}$$

The obvious symmetry property $\rho(\mathbf{n},\mathbf{r}) = \rho(-\mathbf{n},\mathbf{r})$ follows directly. The nematic order in the confining sphere will be described by using Onsager's method[39−41] to each small volume element having a constant director. In addition, the free energy functional of Onsager has to be generalized to include (i) a spatial dependence, (ii) a term representing the entropy penalty connected with the spatial inhomogeneities appearing inside the sphere, and (iii) a term introducing the impenetrable spherical surface. Finally, the extended free energy functional has to be integrated over the volume of the confining sphere. Thus, the free energy density functional for a semiflexible polymer confined in a sphere is expressed by[44,46,47]

$$\begin{aligned}\frac{F[\rho]}{k_BT} = &-\int\int \mathrm{d}\mathbf{r}\,\mathrm{d}\mathbf{n}\;\psi(-\mathbf{n},\mathbf{r})\Delta_{\mathbf{n}}\psi(\mathbf{n},\mathbf{r}) + \\ &l_p\int\int \mathrm{d}\mathbf{r}\,\mathrm{d}\mathbf{n}\;\psi(-\mathbf{n},\mathbf{r})(\mathbf{n}\cdot\nabla_{\mathbf{r}})\psi(\mathbf{n},\mathbf{r}) + \\ &l_p^2 d\int\int\int \mathrm{d}\mathbf{r}\,\mathrm{d}\mathbf{n}\,\mathrm{d}\mathbf{n}'\;\rho(\mathbf{n},\mathbf{r})\rho(\mathbf{n}',\mathbf{r})\sin\gamma_{\mathbf{nn}'} + \\ &\mu\left[\int\int \mathrm{d}\mathbf{n}\,\mathrm{d}\mathbf{r}\;\rho(\mathbf{n},\mathbf{r}) - \frac{L}{l_p}\right] + \lambda\int \mathrm{d}\mathbf{n}\mathrm{d}\mathbf{r}\;\rho(\mathbf{n},\mathbf{r})\Big|_{r=R}\end{aligned} \tag{2}$$

The first term represents the entropy losses connected with orientational inhomogeneities.[39−41] Here and in other terms, the spatial integration is over the volume of the confining sphere according to $\int \mathrm{d}\mathbf{r} \equiv \int\int\int r^2 \sin\Theta\,\mathrm{d}r\,\mathrm{d}\Theta\,\mathrm{d}\Phi$, obtained as the limit of the summation over the small volume elements with constant director $\mathbf{u}$ (see Figure 1), and the orienta-

tional integration is over the unit sphere according to $\int d\mathbf{n} \equiv \int\int \sin\theta \, d\theta \, d\phi$. The second term is related to spatial segment inhomogeneities and can be derived, as well as the first term, from a general theory by Lifshitz,[45] which describes entropy losses from any kind of inhomogeneities in the system (see Appendix A). The third term denotes the steric interaction described through the second virial approximation.[39−41] The last two terms introduce the conditions of constant amount of segments in the sphere and impenetrability of the spherical surface for the polymer segments, respectively, where μ and λ are Lagrange multipliers. The last term implies zero polymer segment density at the surface.

Our aim is now to minimize the free energy functional $F[\rho]$ given by eq 2 with respect to the generalized density function $\rho(\mathbf{n},\mathbf{r})$. A standard way to minimize a functional such as $F[\rho]$ is to use a variational ansatz, which transforms the minimization of the functional into a minimization of a function. For this purpose, let us choose the wave function $\psi(\mathbf{n},\mathbf{r})$ and thus the generalized density $\rho(\mathbf{n},\mathbf{r})$ in the form of trial functions, which explicitly depend on $\mathbf{n}$ and $\mathbf{r}$. This will be made in two subsequential steps.

First, the $\mathbf{n} = (\theta,\phi)$ dependence of $\psi(\mathbf{n},\mathbf{r})$ and $\rho(\mathbf{n},\mathbf{r})$ is expanded in the complete space formed by the spherical harmonics $Y_{lm}(\mathbf{n})$,[48] while the coefficients of the expansions are $\mathbf{r}$ dependent, according to

$$\psi(\mathbf{n},\mathbf{r}) = \sum_{l,m} q_{lm}(\mathbf{r}) Y_{lm}(\mathbf{n}) \tag{3}$$

$$\rho(\mathbf{n},\mathbf{r}) = \sum_{l,m} f_{lm}(\mathbf{r}) Y_{lm}(\mathbf{n}) \tag{4}$$

Here, and in the following, the simplifying notation $\sum_{l,m} \equiv \sum_{l=0}^{\infty}\sum_{m=-l}^{l}$ is used. The spherical harmonics satisfy the orthogonality condition given by

$$\int d\mathbf{n} \, Y_{l_1 m_1}(\mathbf{n}) Y^*_{l_2 m_2}(\mathbf{n}) = \delta_{l_1 l_2}\delta_{m_1 m_2} \tag{5}$$

where * denotes a complex conjugate. Furthermore, for the sake of simplicity, let us assume that the coefficients $q_{lm}(\mathbf{r})$ and $f_{lm}(\mathbf{r})$ in eqs 3 and 4 are real according to

$$\begin{aligned} q_{lm}(\mathbf{r}) &= q^*_{lm}(\mathbf{r}) = (-1)^m q_{l-m}(\mathbf{r}) \\ f_{lm}(\mathbf{r}) &= f^*_{lm}(\mathbf{r}) = (-1)^m f_{l-m}(\mathbf{r}) \end{aligned} \tag{6}$$

After the substitution of eqs 3 and 4 into eq 2, the variables $\mathbf{r}$ and $\mathbf{n}$ are separable. Furthermore, the integrals over $\mathbf{n}$ become analytic. Details of the integration of the free energy functional are given in Appendix B. The final result becomes

$$\begin{aligned} \frac{F[\rho]}{k_B T} = & \int d\mathbf{r} \sum_{l,m} (-1)^l l(l+1)[q_{lm}(\mathbf{r})]^2 + \\ & l_p\sqrt{\frac{2\pi}{3}} \int d\mathbf{r} \sum_{l_1,m_1}\sum_{l_2,m_2} (-1)^{l_1} \times \\ & \Bigg[(I_{1-1l_1m_1l_2m_2} - I_{11l_1m_1l_2m_2}) q_{l_1m_1}(\mathbf{r}) \frac{\partial q_{l_2m_2}(\mathbf{r})}{\partial r} + \\ & i(I_{1-1l_1m_1l_2m_2} + I_{11l_1m_1l_2m_2}) \frac{q_{l_1m_1}(\mathbf{r})}{r} \frac{\partial q_{l_2m_2}(\mathbf{r})}{\partial \Theta} + \\ & \sqrt{2} I_{10l_1m_1l_2m_2} \frac{q_{l_1m_1}(\mathbf{r})}{\sin\Theta} \frac{\partial q_{l_2m_2}(\mathbf{r})}{\partial \Phi} \Bigg] + \\ & l_p{}^2 d \int d\mathbf{r} \sum_{l=0}^{\infty} \sum_{m=-2l}^{2l} \frac{4\pi d_{2l}}{4l+1} [f_{2lm}(\mathbf{r})]^2 + \\ & \mu \Bigg[\int d\mathbf{r} \sum_{l,m} (-1)^l (q_{lm}(\mathbf{r}))^2 - \frac{L}{l_p} \Bigg] + \\ & \lambda R^2 \iint d\Theta d\Phi \ \sin\Theta \sum_{l,m} (-1)^l [q_{lm}(R,\Theta,\Phi)]^2 \end{aligned} \tag{7}$$

where the following notation is used

$$I_{l_1m_1l_2m_2l_3m_3} = \int d\mathbf{n} \, Y_{l_1m_1}(\mathbf{n}) Y_{l_2m_2}(\mathbf{n}) Y_{l_3m_3}(\mathbf{n}) \tag{8}$$

and

$$d_{2l} = -\frac{\pi(4l+1)(2l)!(2l-2)!}{2^{4l+1}(l-1)!l!l!(l+1)!} \tag{9}$$

and where the coefficients $f_{lm}(\mathbf{r})$ are related to $q_{lm}(\mathbf{r})$ through

$$f_{lm}(\mathbf{r}) = \sum_{l,m_1}\sum_{l_2,m_2} (-1)^{l_1+m} I_{l-ml_1m_1l_2m_2} q_{l_1m_1}(\mathbf{r}) q_{l_2m_2}(\mathbf{r}) \tag{10}$$

Equation 7 shows that the dependence on $\mathbf{n}$ in eq 2 is eliminated and that the free energy expression becomes a functional of the $\mathbf{r}$-dependent coefficients $q_{lm}(\mathbf{r})$.

The second step involves the assignment of another trial function describing the $\mathbf{r}$ dependence of the coefficients $q_{lm}(\mathbf{r})$. Obviously, the assumption of cylindrical symmetric director makes the generalized density $\rho(\mathbf{r})$ independent of Φ. Since $\rho(\mathbf{r}) \sim \psi^2(\mathbf{r}) \sim q_{lm}{}^2(\mathbf{r})$, the coefficients $q_{lm}(\mathbf{r})$ also possess cylindrically symmetric, i.e., $q_{lm}(\mathbf{r}) = q_{lm}(r,\Theta)$. A simple way to introduce the dependence of q_{lm} on r and Θ is to use a power series for r and the Legendre polynomial series $P_{2j}(\cos\Theta)$ for Θ according to

$$q_{lm}(\mathbf{r}) = q_{lm}(r,\Theta) = \sum_{i,j} C_{lmij} \left(\frac{r}{R}\right)^i P_{2j}(\cos\Theta) \tag{11}$$

with C_{lmij} being the expansion coefficients. Here, the expansion with respect to even Legendre polynomials only reflects the inversion symmetry of physical properties in the system, i.e., the polymer density and order are symmetrical about the equatorial plane of the sphere. Substitution of eq 11 in eq 7 and subsequent analytic integration over $\mathbf{r}$ result in a free energy function depending only on the C_{lmij} coefficients.

Here, indices l and m are connected with orientational degrees of freedom, whereas i and j with the spatial ones. Finally, the minimizing of the multivariable free energy function with respect to the coefficients C_{lmij} provides $q_{lm}(\mathbf{r})$, and, hence, the corresponding generalized density $\rho(\mathbf{n},\mathbf{r})$ represents the variational minimum of the free energy functional given by (2). In Appendix C, we discuss the truncations of the expansions of the orientation and segment distributions made in eqs 3 and 11, respectively.

Having the generalized density $\rho(\mathbf{n},\mathbf{r})$, the spatial-dependent polymer volume fraction $\varphi(\mathbf{r})$ inside the sphere is obtained by integrating $\rho(\mathbf{n},\mathbf{r})$ over the orientational degrees of freedom according to

$$\varphi(\mathbf{r}) = \frac{\pi d^2}{4} l_p \int d\mathbf{n}\, \rho(\mathbf{n},\mathbf{r}) = \frac{\pi d^2}{4} l_p \sqrt{4\pi} f_{00}(\mathbf{r}) \quad (12)$$

The spatial dependence of the order parameter in the confining sphere can be found using $\rho(\mathbf{n},\mathbf{r})$ as a weight average of the order tensor $(3\mathbf{n}_\alpha\mathbf{n}_\beta - \mathbf{I}_{\alpha\beta})/2$ according to

$$S_{\alpha\beta}(\mathbf{r}) = \frac{\frac{1}{2}\int d\mathbf{n}\,(3\mathbf{n}_\alpha\mathbf{n}_\beta - \mathbf{I}_{\alpha\beta})\rho(\mathbf{n},\mathbf{r})}{\int d\mathbf{n}\,\rho(\mathbf{n},\mathbf{r})}, \quad (\alpha,\beta) = (x,y,z) \quad (13)$$

It can be shown that the matrix of the tensor after diagonalization is traceless and has the form:

$$\mathbf{S}_{\alpha\alpha}(\mathbf{r}) = \begin{pmatrix} \frac{1}{2}[B(\mathbf{r}) - S(\mathbf{r})] & 0 & 0 \\ 0 & -\frac{1}{2}[B(\mathbf{r}) + S(\mathbf{r})] & 0 \\ 0 & 0 & S(\mathbf{r}) \end{pmatrix} \quad (14)$$

Here, $B(\mathbf{r})$ is the parameter indicating appearance of biaxiality in the system (biaxiality parameter); $B(\mathbf{r}) = 0$ corresponds to the uniaxial nematic order. Generally speaking, a nematic liquid crystal in contact with surface is always biaxial,[43,49,50] $B(\mathbf{r}) \neq 0$; i.e., it can be aligned not only parallel but also perpendicular to the surface. A nematic director, $\mathbf{u}$, can be defined as the eigenvector corresponding to the largest eigenvalue $S(\mathbf{r})$ of the tensor $S_{\alpha\beta}(\mathbf{r})$. In our work, we restrict ourselves by only consideration of the nematic order with the largest eigenvalue $S(\mathbf{r})$ and corresponding eigenvector $\mathbf{u}$, which is supposed to be the main contribution to the total nematic order in the system. Physically, this main contribution corresponds to the situation when the conformation of the polymer inside the sphere has a cylindric symmetry; i.e., the polymer is aligned parallel to the surface of the sphere.

3. Results and Discussion

We will focus throughout on systems where the radius of the confining sphere R is 20 times the diameter of the

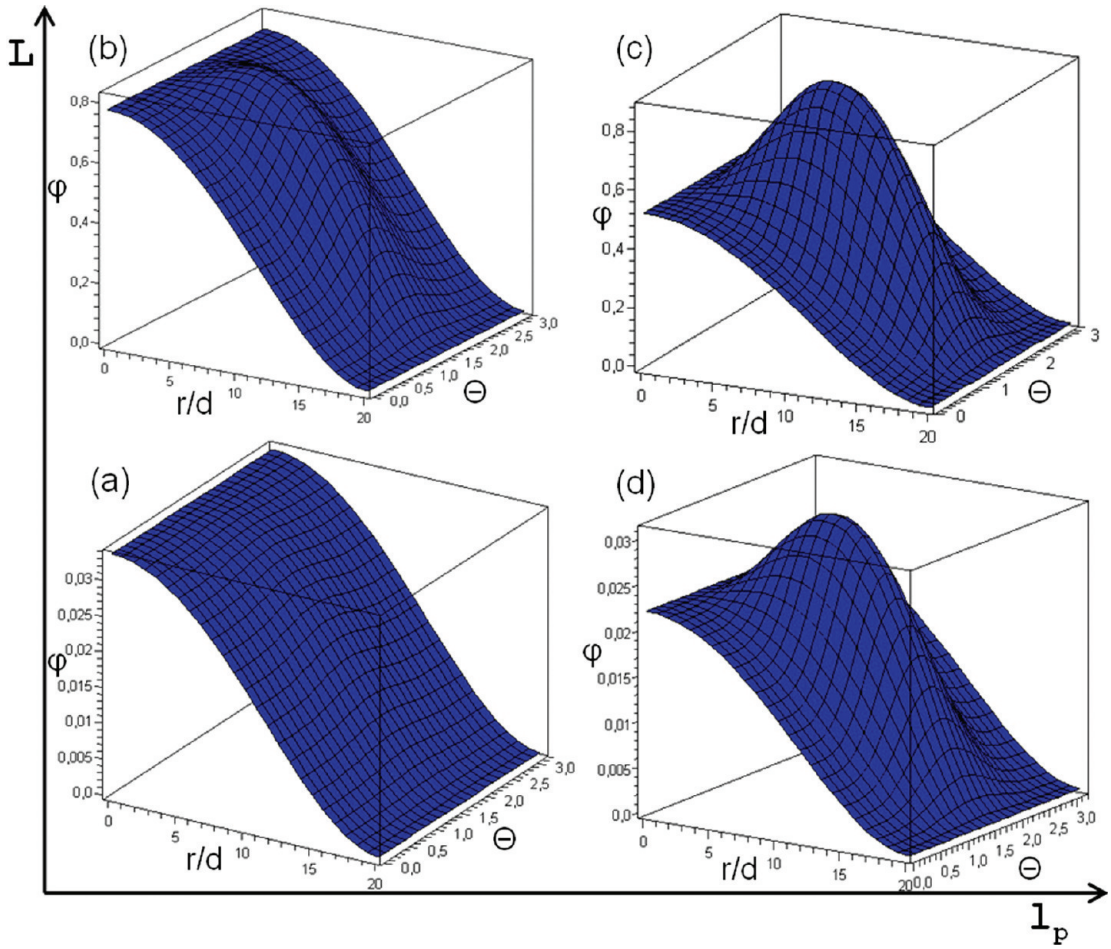

Figure 2. Polymer volume fraction φ vs the scaled radial distance r and the azimuthal angle Θ (in radians) for (a) $L = 363d$, $l_p = 10d$, (b) $L = 10^4 d$, $l_p = 10d$, (c) $L = 10^4 d$, $l_p = 50d$, and (d) $L = 363d$, $l_p = 50d$ at the sphere radius $R = 20d$.

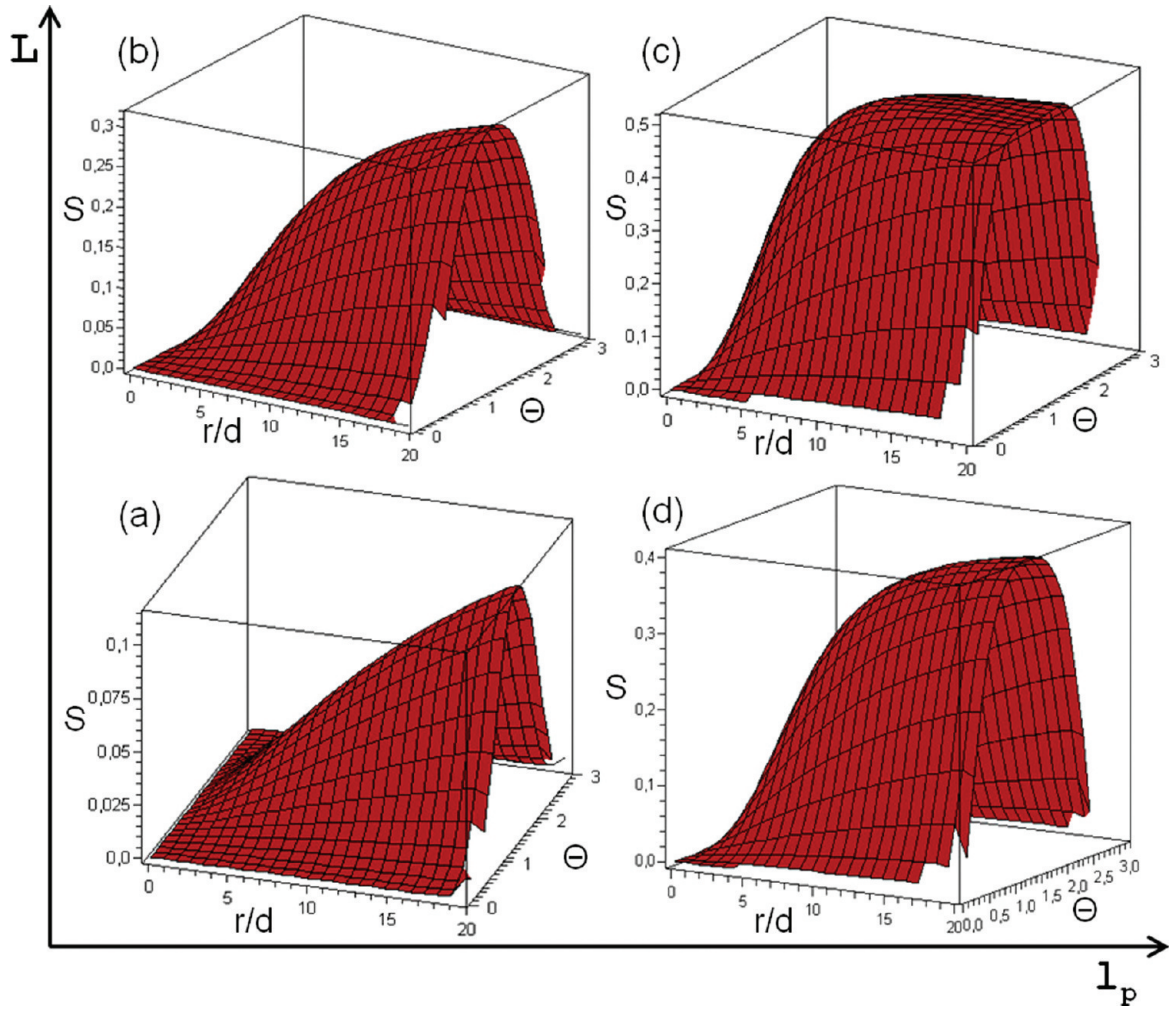

Figure 3. Orientational order parameter S vs the scaled radial distance to r and the azimuthal angle Θ (in radians) for (a) $L = 363d$, $l_p = 10d$, (b) $L = 10^4d$, $l_p = 10d$, (c) $L = 10^4d$, $l_p = 50d$, and (d) $L = 363d$, $l_p = 50d$ at the sphere radius $R = 20d$.

polymers. With a DNA diameter of $d = 2$ nm, that would correspond to a typical viral capsid radius of $R = 40$ nm. Our first set of results will cover four different combinations of short ($L = 363d$) and long ($L = 10^4d$) contour lengths with less ($l_p = 10d$) and more ($l_p = 50d$) rigid polymers relevant to experimental observations.[51] Thus, the shorter polymer has a contour length ca. 3 times the circumference of the confining sphere and the longer one is ca. 80 times the circumference. The less rigid polymer has a persistence length half of the radius of the confining sphere and the more rigid one 2.5 times the radius.

Three-dimensional graphs of polymer volume fraction $\varphi(\mathbf{r}) = \varphi(r/d,\Theta)$ are given in Figure 2 and of orientational order parameter $S(\mathbf{r}) = S(r/d,\Theta)$ are given in Figure 3 as functions of the scaled radial distance r/d from the center of the confining sphere and the azimuthal angle Θ for the four types of polymers. The horizontal l_p and vertical L arrows indicate the directions of increasing persistence and contour lengths, respectively.

Regarding the short and less rigid polymer, the maximal density appears at $r/d = 0$ and no angular dependence is found (Figure 2a). The orientational order vanishes at the center and grows to $S \approx 0.1$ at the surface, which indicates a small but nonzero induced order near the surface (Figure 3a). A 30-fold increase of the polymer contour length (i) shifts the density maximum toward the surface of the confining sphere and (ii) breaks the isotropic density distribution with respect to the azimuthal angle Θ (Figure 2b). The spatial dependence of the order parameters remains the same, though the maximal order parameter near the surface becomes $S \approx 0.25$. However, a 5-fold increase of the polymer persistence length has an even larger impact. Though the overall segment density in the confining sphere is low (on the average $\varphi = (3/16)d^2L/R^3 = 0.0085$, the maximal polymer density is found in a distinct annular volume with radius $r/d \approx 8$ (Figure 2d). The predicted orientational order increases radially and attains its maximum still at the confining surface at $\Theta = \pi/2$. The combination of a longer contour length and stiffer polymer gives rise to the largest inhomogeneous segment distribution (Figure 2c) and to a homogeneous orientational order from $r/d \approx 8$ at the equatorial plane and near the surface, and the region of high order extends further to the poles than in the previous cases (Figure 3c).

Thus, we observe that increasing (i) the effective repulsion between polymer segments by increasing the segment density inside the sphere and/or (ii) the persistence length of the polymers the density maximum appearing in the center of the sphere is shifted to an annular region (density maximum at $r/d > 0$ and $\Theta = \pi/2$) and the orientational order is increased. The effect of increasing the persistence length 5-fold is larger than

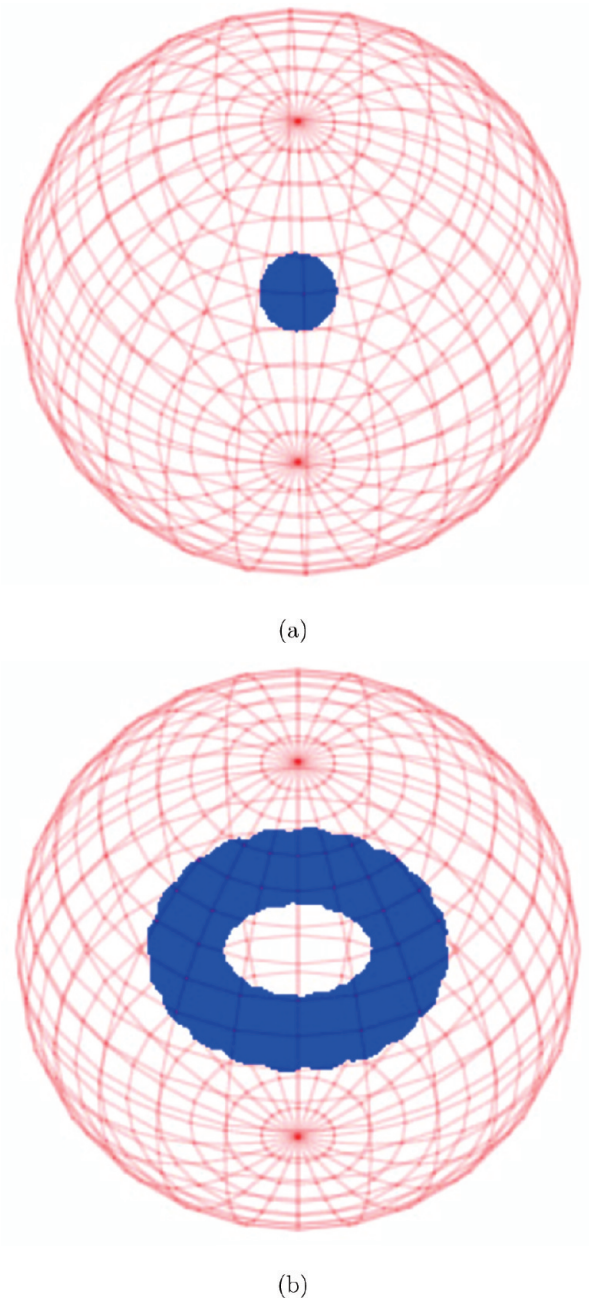

Figure 4. Schematic picture of polymer distribution inside the sphere of radius $R = 20d$ for (a) $L = 363d$, $l_p = 10d$, and (b) $L = 10^4d$, $l_p = 50d$. The blue regions represent locations in which the polymer density is at least 99% of the maximal one.

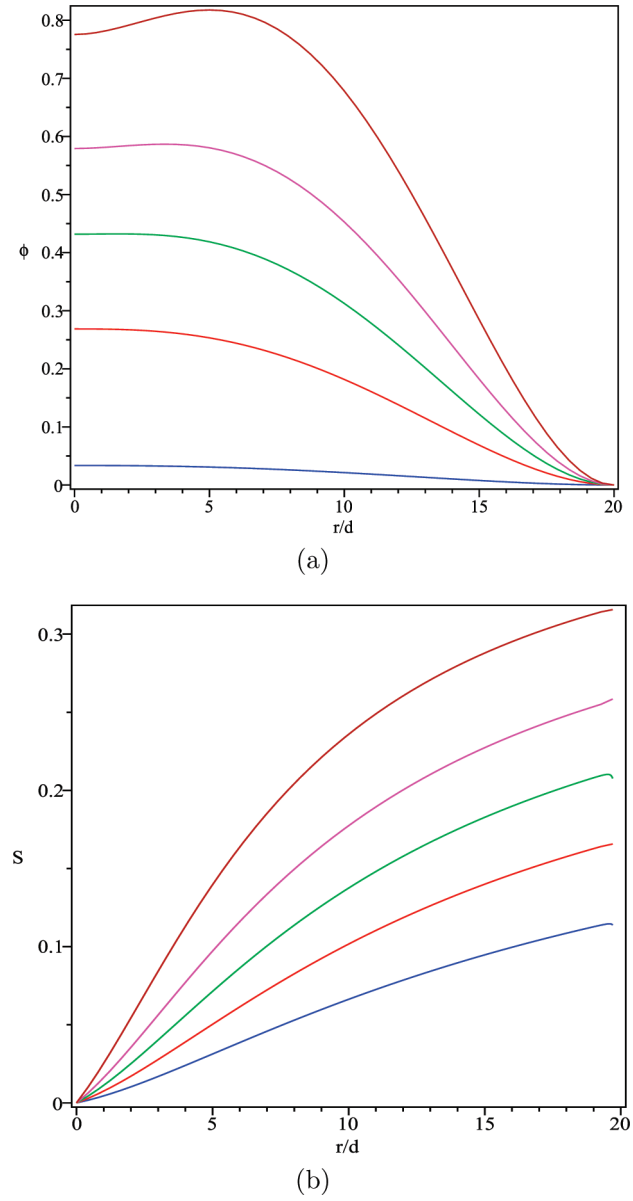

Figure 5. (a) Polymer volume fraction φ and (b) orientational order parameter S vs the radial distance r at $\Theta = \pi/2$ (the equatorial plane of the confining sphere) for polymer contour length $L = 363d$ (blue), $L = 3000d$ (red), $L = 5000d$ (green), $L = 7000d$ (magenta), $L = 10^4d$ (brown) at the polymer persistence length $l_p = 10d$, and the sphere radius $R = 20d$.

that of a 30-fold density increase. Obviously, the elastic energy of the chain is an important factor for arranging a toroidal density distribution. The toroidal segment distribution is interpreted as a toroidal polymer conformation, which has a lower bending energy than a coil conformation. The segment orientational order is also obviously increased with increasing density and/or persistence length, again with stronger effect at increasing persistence length.

A rough idea of how the polymer is distributed inside the sphere can be seen from Figure 4a,b illustrating the regions of predominant polymer location for two limiting situations. Figure 4 corresponds to the case of short and less rigid polymer (see also Figure 2a), while Figure 4b illustrates the conformation of a stiffer polymer having a longer contour length (see Figure 2c). Obviously, the former conformation resembles a disordered coil, while the latter is similar to a torus. One has to note that the blue regions in Figure 4a,b mark the areas where the polymer predominantly appears, and cannot be considered as an entire polymer concentration map. In fact, there is a nonzero polymer concentration everywhere in the sphere except at the surface (Figure 2, a and c).

We will now in more detail examine the radial dependence of the polymer volume fraction and the orientational order parameter at the equatorial plane at increasing contour length at the persistence length $l_p = 10d$ (Figure 5, a and b) and at increasing persistence length starting with $l_p = d$ at the contour length $L = 10^4d$ (Figure 6, a and b). Figure 5a shows that at the persistence length $l_p = 10d$ density maximum appears at

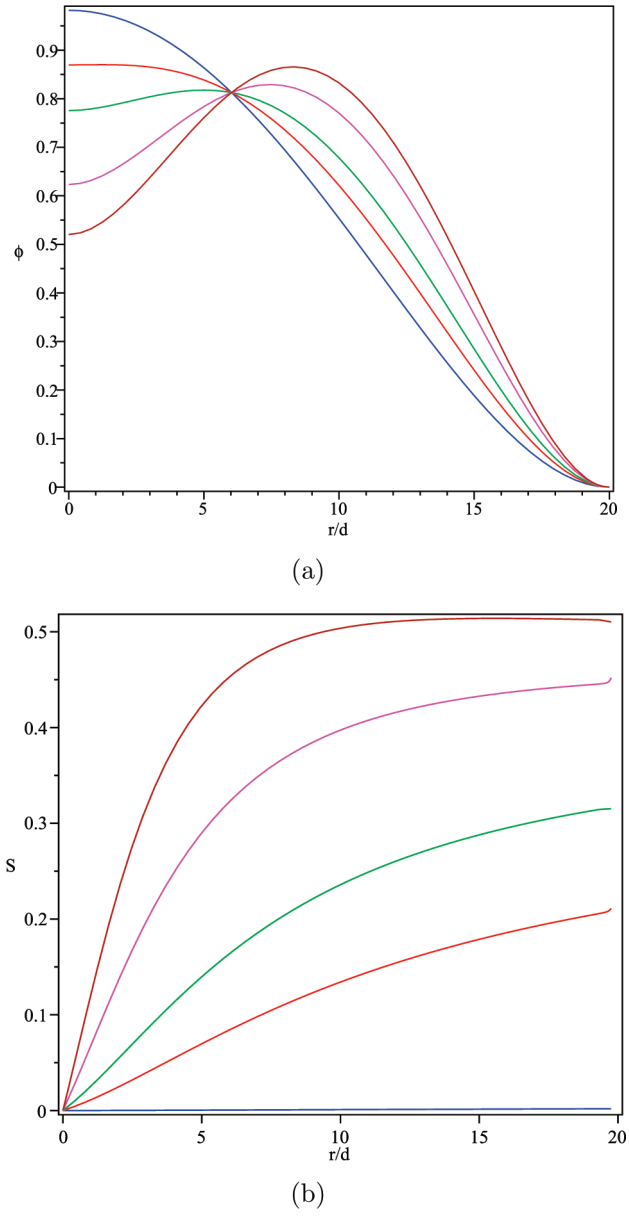

Figure 6. (a) Polymer volume fraction φ and (b) orientational order parameter S vs the radial distance r at $\Theta = \pi/2$ (the equatorial plane of the confining sphere) for polymer persistence length $l_p = d$ (blue), $l_p = 7d$ (red), $l_p = 10d$ (green), $l_p = 20d$ (magenta), $l_p = 50d$ (brown) at the polymer contour length $L = 10^4 d$, and the sphere radius $R = 20d$.

the center of the sphere up to $L \approx 6000d$ and thereafter it is shifted off the center. The polymer density is fairly constant for $r/d < 10$, though the level is increasing with polymer contour length. Figure 5b shows that the corresponding orientational order increases radially with increasing contour length in a regular fashion. This effect is qualitatively confirmed by recent cryo-EM measurements indicating the phase transition from the hexagonally packed structure to the isotropic one upon the DNA ejection from the T5 virus.[8]

Figure 6, a and b, shows the radial polymer volume fraction and the orientational order parameter for long ($L = 10^4 d$) polymers ranging from flexible ($l_p = d$) to rigid ($l_p = 50d$) ones. There is a clear displacement of the polymer from the center of the sphere upon the increasing persistence length, which is in excellent agreement with the recent results of computer simulations.[52] Furthermore, the order parameter is below 0.01 for the most flexible polymer ($l_p = d$) and increases continuously with increasing persistence length. The nearly constant orientational order over an extended radial range starting at $r/d \approx 10$ at the persistence length $l_p = 50d$ is clearly visible.

An interesting observation deduced from Figures 2, 5a, and 6a is that the polymer never leaves completely the center of the capsid, as it would be favorable from the point of view of elasticity energy. To explain this, one has to realize that the density distribution is always a result of a balance between elasticity energy and the energy of steric interactions. The latter favor a uniform density distribution and counterbalance the tendency of the polymer to be fully aligned at the surface. Furthermore, comparing Figures 2, 5a, and 6a and Figures 3, 5b, and 6b, respectively, one can notice that despite the presence of the polymer in the center, the order parameter $S(\mathbf{r})$ surprisingly is equal to zero at $r = 0$. This effect is a direct consequence of biaxiality in the system. Here we have to emphasize that $S(r{=}0) = 0$ does not imply the absence of any order in the center, but simply indicates the absence of the order with cylindrical symmetry, which is considered as a main contribution. Due to biaxiality, the polymer in the center can be equally well aligned perpendicular to the equatorial plane of the sphere, but this contribution is not captured by the order parameter $S(\mathbf{r})$ used; here $B(r{=}0) \neq 0$ and $S(r = 0) = 0$. Recall that we postulate the order to be cylindrically symmetric, which means that the axis $r = 0$ is a singularity axis for the director field. Interestingly, our result seems to be in a good agreement with cryo-TEM experiments[4−8] indicating the presence of disordered polymer in the center of capsid. The parameters (contour length, capsid radius, average volume fraction) chosen for the Figure 2c are very close to those for the bacteriophages $\phi 29$ and T7 observed in experiments.[4,5,51] Thus, Figures 2c and 4b provide the picture of how DNA is arranged inside these real viruses.

The realization of hard surfaces in polymer density functional theories (as here) typically leads to zero polymer segment density at the surface, which is in agreement with some experiments.[53] However, simulations using coarse-grained or atomistic models typically display nonzero polymer segment densities at the surface. Hence, the zero polymer segment density at the spherical surface is a consequence of the implementation of the confinement in the current theory, and consequently the polymer segment density very close to the spherical surface should not be taken too literal.

Another interesting result is the apparent absence of a discontinuity of the order parameter upon increasing contour and persistence lengths, which indicates that the phase transition in the sphere is second-order-like. It is known[54] that a gradual increase of the order parameter corresponds to the case of strong external field. Thus, we can conclude that genome compressed in a spherical cavity behaves similar to a polymer with excluded volume interaction in a strong external field.

We emphasize that all the effects discussed in the present paper were predicted without electrostatic forces being involved. This obviously does not fully correspond to viral systems as both genome and capsid are charged. Nevertheless, the formalism used here should be applicable for weakly charged systems or systems with high salt content. Moreover, our theory brings a new fundamental insight into the problem, since it can be considered as a first step to investigate the capsids from the nematic order point of view. Electrostatic

effects will enrich the behavior of the system and can be included into our theory within the frameworks of similar formalism.[55,56] To first order, the electrostatic interaction could be included in the effective second virial approximation. In such a way, we expect the nematic order transition to be more pronounced for charged confined polymers.

4. Conclusions

We proposed a new approach to the investigation of conformation of a double-stranded DNA inside a spherical viral capsid. The main idea of the present theory is to consider the arrangement of DNA in the capsid as a simple nematic liquid crystal and apply the Onsager method to this system. The significant difference from the classical theories[39,40] is connected with the constraints of confined geometry; for this purpose, an additional spatial entropy term was added to the inhomogeneous Onsager's free energy functional. The only steric interactions were shown to be enough for demonstration of biaxial nematic order transition in the system upon increase of polymer length and rigidity of the chain. The obtained polymer density and orientational order parameter distributions demonstrate the importance of rigidity of the chain for the nematic order. A short and flexible polymeric chain was shown to be concentrated at the center of the capsid being orientationaly disordered, whereas upon increasing the length and rigidity of the chain, it migrated toward the surface of the capsid locating predominantly at the equator and being highly biaxially ordered. Analyzing the density and order parameter distributions, one can conclude that the conformations of DNA obtained for the case of long and stiff chain resemble the well-known spoollike/torus structure.

Acknowledgment. Financial support by the Swedish Research Council (VR) through the Linnaeus grant for the Organizing Molecular Matter (OMM) Center of Excellence is gratefully acknowledged. N.O. acknowledges Alexander Emelyanenko from the Physics Department of Moscow State University for fruitful discussions. I.I.P and A.R.K. acknowledge the Ministry of Education and Science of Russian Federation for financial support.

Appendix A: Entropy Originating from General Inhomogeneities

This appendix accounts for the leading terms of the entropy contribution to a free energy functional arising from orientational and spatial inhomogeneities. According to Lifshitz,[45] the contribution from the entropy to the free energy functional F depending on the generalized density ρ, which in turn is a function of a generalized coordinate $\mathbf{x}$, can be expressed as

$$\frac{F_{\text{entr}}[\rho]}{k_{\text{B}}T} = -\int \mathrm{d}\mathbf{x}\, \rho(\mathbf{x}) \ln\left(\frac{\hat{g}\psi(\mathbf{x})}{\psi(\mathbf{x})}\right) \tag{15}$$

The wave function $\psi(\mathbf{x})$ entering in eq 15 is related to $\rho(\mathbf{x})$ by $\rho(\mathbf{x}) = \psi(-\mathbf{x})\psi(\mathbf{x})$ and $\hat{g}$ is a microscopic operator with a symmetric core $g(\mathbf{x} - \mathbf{x}') = g(\mathbf{x}' - \mathbf{x})$, which has the meaning of a conditional probability to find the monomeric unit of the chain at the point $\mathbf{x}$ provided that the previous one had coordinate $\mathbf{x}'$, and is given by

$$\hat{g}\psi(\mathbf{x}) = \int g(\mathbf{x} - \mathbf{x}')\psi(\mathbf{x}')\,\mathrm{d}\mathbf{x}' = -\int g(\mathbf{y})\psi(\mathbf{x} - \mathbf{y})\,\mathrm{d}\mathbf{y} = \int g(\mathbf{y})\psi(\mathbf{x} + \mathbf{y})\,\mathrm{d}\mathbf{y} \tag{16}$$

where the distribution function $g(\mathbf{y})$ is assumed to have a Gaussian form and $\int g(\mathbf{y})\,\mathrm{d}\mathbf{y} = 1$ and where the vector $\mathbf{y} = \mathbf{x} - \mathbf{x}'$ defines the inhomogeneities. Assuming that the inhomogeneities are weak, $\psi(\mathbf{x} + \mathbf{y})$ can be expanded into a Taylor series about $\psi(\mathbf{x})$ according to

$$\psi(\mathbf{x} + \mathbf{y}) \approx \psi(\mathbf{x}) + (\mathbf{y}\cdot\nabla_{\mathbf{x}})\psi(\mathbf{x}) + \frac{1}{2}(\mathbf{y}\cdot\nabla_{\mathbf{x}})^2\psi(\mathbf{x}) \tag{17}$$

Hence, the operator eq 16 can be transformed in the following way:

$$\hat{g}\psi(\mathbf{x}) \approx \psi(\mathbf{x})\left[1 + \int g(\mathbf{y})\frac{(\mathbf{y}\cdot\nabla_{\mathbf{x}})\psi(\mathbf{x})}{\psi(\mathbf{x})}\,\mathrm{d}\mathbf{y} + \frac{1}{2}\int g(\mathbf{y})\frac{(\mathbf{y}\cdot\nabla_{\mathbf{x}})^2\psi(\mathbf{x})}{\psi(\mathbf{x})}\,\mathrm{d}\mathbf{y}\right] \tag{18}$$

Moreover, taking into account that $\ln(1 + x) \approx x$, we can express the contribution from the entropy into the free energy according to

$$\frac{F_{\text{entr}}[\rho]}{k_{\text{B}}T} \approx -\int \mathrm{d}\mathbf{x}\left[\int g(\mathbf{y})\psi(-\mathbf{x})(\mathbf{y}\cdot\nabla_{\mathbf{x}})\psi(\mathbf{x})\,\mathrm{d}\mathbf{y} + \frac{1}{2}\int g(\mathbf{y})\psi(-\mathbf{x})(\mathbf{y}\cdot\nabla_{\mathbf{x}})^2\psi(\mathbf{x})\,\mathrm{d}\mathbf{y}\right] \tag{19}$$

where the integration over d$\mathbf{y}$ has a meaning of microscopic statistical averaging with respect to the inhomogeneities.

In our case of orientational and spatial inhomogeneities, the generalized coordinate represents a combination of the tangent vector $\mathbf{n}$ and the radius vector $\mathbf{r}$, hence $\mathbf{x} = \{\mathbf{n},\mathbf{r}\}$, and furthermore the inhomogeneity vector becomes $\mathbf{y} = \mathbf{x} - \mathbf{x}' = \{\mathbf{n} - \mathbf{n}', \mathbf{r} - \mathbf{r}'\} \equiv \{\mathbf{y}_{\mathbf{n}}, \mathbf{y}_{\mathbf{r}}\}$. We will now consider the two terms of eq 19 separately. First, notice that $\langle \mathbf{n} - \mathbf{n}' \rangle \equiv \int g(\mathbf{y}_{\mathbf{n}})\mathbf{y}_{\mathbf{n}}\,\mathrm{d}\mathbf{y}_{\mathbf{n}} = 0$ due to the inversion symmetry of nematic order in bulk approximation, vectors $\mathbf{n} - \mathbf{n}'$ and $\mathbf{n}' - \mathbf{n}$ are equivalent and $g(-\mathbf{y}_{\mathbf{n}}) = g(\mathbf{y}_{\mathbf{n}})$; therefore, the term linear with respect to the orientational gradient $\nabla_{\mathbf{n}}$ becomes zero. On the other hand, vector $\mathbf{r} - \mathbf{r}'$ can be rewritten as $\mathbf{r} - \mathbf{r}' \approx -l_{\text{p}}(\partial\mathbf{r}(s)/\partial s) = -l_{\text{p}}\mathbf{n}$ that provides $\langle \mathbf{r} - \mathbf{r}' \rangle \equiv \int g(\mathbf{y}_{\mathbf{r}})\mathbf{y}_{\mathbf{r}}\,\mathrm{d}\mathbf{y}_{\mathbf{r}} \approx -l_{\text{p}}\mathbf{n} \neq 0$; here s is a coordinate along the chain; hence, the linear spatial gradient $\nabla_{\mathbf{r}}$ becomes nonzero and $\langle \mathbf{y}\cdot\nabla_{\mathbf{x}} \rangle = -l_{\text{p}}(\mathbf{n}\cdot\nabla_{\mathbf{r}})$ gives the second term of eq 2. In analogy, the second term of eq 19 gives rise to orientational and spatial Laplacians, $\Delta_{\mathbf{n}} \equiv \nabla_{\mathbf{n}}^2$ and $\Delta_{\mathbf{r}} \equiv \nabla_{\mathbf{r}}^2$, respectively, since

$\mathbf{n}$ and $\mathbf{y_n} = \mathbf{n} - \mathbf{n}'$ are unit vectors and therefore $\int g(\mathbf{y_n})\mathbf{y_n}^2\, d\mathbf{y_n} = 1$, $\int g(\mathbf{y_r})\mathbf{y_r}^2\, d\mathbf{y_r} \sim l_p^2$. Finally, by retaining only the first nonzero terms with respect to orientation and spatial inhomogeneities in eq 19, the first and the second terms in the free energy functional (2) are obtained.

Appendix B: Integration of Free Energy Functional

More details of the derivation of the free energy functional given by eq 7 is provided in this appendix. Equation 7 is obtained by substitution of the expansions given by eqs 3 and 4 into eq 2 with a subsequent integration over the orientational variable $\mathbf{n} = (\theta,\phi)$.

The first term of eq 7 is obtained by recognizing that the spherical harmonic $Y_{lm}(\mathbf{n})$ is an eigenfunction of the Laplace operator according to $\Delta_{\mathbf{n}} Y_{lm}(\mathbf{n}) = -l(l+1)Y_{lm}(\mathbf{n})$ with $-l(l+1)$ being its eigenvalue. Hence

$$
\begin{aligned}
&-\int\int d\mathbf{r}\, d\mathbf{n}\, \psi(-\mathbf{n},\mathbf{r})\Delta_{\mathbf{n}}\psi(\mathbf{n},\mathbf{r}) \\
&= -\int\int d\mathbf{r}\, d\mathbf{n}\left[\sum_{l_1,m_1}(-1)^{l_1} q_{l_1m_1}(\mathbf{r})Y_{l_1m_1}(\mathbf{n})\right]\left[\sum_{l,m} q_{lm}(\mathbf{r})\Delta_{\mathbf{n}}Y_{lm}(\mathbf{n})\right] \\
&= \int\int d\mathbf{r}\, d\mathbf{n}\left[\sum_{l_1,m_1}(-1)^{l_1} q_{l_1m_1}(\mathbf{r})Y_{l_1m_1}(\mathbf{n})\right]\left[\sum_{l,m} q_{lm}(\mathbf{r})l(l+1)Y_{lm}(\mathbf{n})\right] \\
&= \int d\mathbf{r}\left[\sum_{l_1,m_1}\sum_{l,m}(-1)^{l_1+m} l(l+1)q_{lm}(\mathbf{r})q_{l_1m_1}(\mathbf{r})\right]\int d\mathbf{n}\, Y_{l_1m_1}(\mathbf{n})Y^*_{l-m}(\mathbf{n}) \\
&= \int d\mathbf{r}\sum_{l,m}(-1)^{l+m} l(l+1)q_{lm}(\mathbf{r})q_{l-m}(\mathbf{r}) \\
&= \int d\mathbf{r}\sum_{l,m}(-1)^{l} l(l+1)[q_{lm}(\mathbf{r})]^2
\end{aligned}
\tag{20}
$$

where the orthogonality condition for spherical harmonics given by eq 5 and the restriction given by eq 6 have been used. The first term, $l = 0$, corresponds to an isotropic state of the system, where the orientational entropy is zero.

To integrate the second term of eq 2, representing the entropy losses due to spatial inhomogeneities, one has first to simplify the scalar product $(\mathbf{n}\cdot\nabla_{\mathbf{r}})$. The vectors $\mathbf{n}$ and $\nabla_{\mathbf{r}}$ are specified in the coordinate systems $(\hat{n}_x,\hat{n}_y,\hat{n}_z)$ and $(\hat{r},\hat{\Theta},\hat{\Phi})$, respectively, where quantities with a hat denote basis vectors. From our assumption of cylindrical symmetry of the director field, the coordinate system $(\hat{n}_x,\hat{n}_y,\hat{n}_z)$ is oriented such that $\hat{n}_z = \hat{\Phi}$. Furthermore, for the sake of simplicity, let the two remaining coordinate axes $\hat{n}_x$ and $\hat{n}_y$ coincide with $\hat{r}$ and $\hat{\Theta}$, respectively. A more rigorous calculation of the scalar product $(\mathbf{n}\cdot\nabla_{\mathbf{r}})$ can be done using the Euler angles,[48] which are expected to only change coefficients in the final expression of the scalar product without influencing the qualitative picture of the nematic order in the system. Furthermore, the tangent vector $\mathbf{n} = (\sin\theta\cos\phi, \sin\theta\sin\phi, \cos\theta)$ is rewritten through the spherical harmonics according to

$$
\begin{aligned}
\sin\theta\cos\phi &= \sqrt{\frac{2\pi}{3}}[Y_{1-1}(\mathbf{n}) - Y_{11}(\mathbf{n})] \\
\sin\theta\sin\phi &= i\sqrt{\frac{2\pi}{3}}[Y_{1-1}(\mathbf{n}) + Y_{11}(\mathbf{n})] \\
\cos\theta &= \sqrt{\frac{4\pi}{3}}Y_{10}(\mathbf{n})
\end{aligned}
\tag{21}
$$

Finally, representing the gradient vector $\nabla_{\mathbf{r}}$ in the cylindrical coordinate system according to

$$
\nabla_{\mathbf{r}} = \left(\frac{\partial}{\partial r}, \frac{1}{r}\frac{\partial}{\partial\Theta}, \frac{1}{\sin\Theta}\frac{\partial}{\partial\Phi}\right)
$$

the second term in eq 2 can be expressed as

$$
\begin{aligned}
&l_p\int\int d\mathbf{r}\, d\mathbf{n}\, \varphi(-\mathbf{n},\mathbf{r})(\mathbf{n}\cdot\nabla_{\mathbf{r}})\psi(\mathbf{n},\mathbf{r}) \\
&= l_p\int\int d\mathbf{r}\, d\mathbf{n}\left[\sum_{l_1,m_1}(-1)^{l_1} q_{l_1m_1}(\mathbf{r})Y_{l_1m_1}(\mathbf{n})\right]\times \\
&\qquad (\mathbf{n}\cdot\nabla_{\mathbf{r}})\left[\sum_{l_2,m_2} q_{l_2m_2}(\mathbf{r})Y_{l_2m_2}(\mathbf{n})\right] \\
&= l_p\int d\mathbf{r}\sum_{l_1,m_1}\sum_{l_2,m_2}(-1)^{l_1}\left[q_{l_1m_1}(\mathbf{r})\frac{\partial q_{l_2m_2}(\mathbf{r})}{\partial r}\times\right. \\
&\qquad \int d\mathbf{n}\sqrt{\frac{2\pi}{3}}[Y_{1-1}(\mathbf{n}) - Y_{11}(\mathbf{n})]\times Y_{l_1m_1}(\mathbf{n})Y_{l_2m_2}(\mathbf{n}) + \\
&\qquad \frac{q_{l_1m_1}(\mathbf{r})}{r}\frac{\partial q_{l_2m_2}(\mathbf{r})}{\partial\Theta}\int d\mathbf{n}\, i\sqrt{\frac{2\pi}{3}}[Y_{1-1}(\mathbf{n}) - Y_{11}(\mathbf{n})]\times \\
&\qquad Y_{l_1m_1}(\mathbf{n})Y_{l_2m_2}(\mathbf{n}) + \frac{q_{l_1m_1}(\mathbf{r})}{\sin\Theta}\frac{\partial q_{l_2m_2}(\mathbf{r})}{\partial\Phi}\times \\
&\qquad \left.\int d\mathbf{n}\sqrt{\frac{4\pi}{3}}Y_{10}(\mathbf{n})Y_{l_1m_1}(\mathbf{n})Y_{l_2m_2}(\mathbf{n})\right] \\
&= l_p\sqrt{\frac{2\pi}{3}}\int d\mathbf{r}\sum_{l_1,m_1}\sum_{l_2,m_2}(-1)^{l_1}[(I_{1-1l_1m_1l_2m_2} - I_{11l_1m_1l_2m_2})\times \\
&\qquad q_{l_1m_1}(\mathbf{r})\frac{\partial q_{l_2m_2}(\mathbf{r})}{\partial r} + i(I_{1-1l_1m_1l_2m_2} + I_{11l_1m_1l_2m_2})\times \\
&\qquad \left.\frac{q_{l_1m_1}(\mathbf{r})}{r}\frac{\partial q_{l_2m_2}(\mathbf{r})}{\partial\Theta} + \sqrt{2}I_{10l_1m_1l_2m_2}\frac{q_{l_1m_1}(\mathbf{r})}{\sin\Theta}\frac{\partial q_{l_2m_2}(\mathbf{r})}{\partial\Phi}\right]
\end{aligned}
\tag{22}
$$

where the constant $I_{l_1m_1l_2m_2l_3m_3}$ is given by eq 8.

The third term in eq 7 represents the steric interactions in the system and can be derived in a similar manner as the previous ones. First, using the addition theorem for spherical harmonics,[48] the angle $\gamma_{\mathbf{nn}'}$ between two interacting segments with tangent vectors $\mathbf{n}$ and $\mathbf{n}'$ can be expressed as

$$
\sin\gamma_{\mathbf{nn}'} = \sum_{l=0}^{\infty}\sum_{m=-2l}^{2l}\frac{4\pi d_{2l}}{4l+1}Y_{2lm}(\mathbf{n})Y^*_{2lm}(\mathbf{n}')
\tag{23}
$$

where

$$
d_{2l} = -\frac{\pi(4l+1)(2l)!(2l-2)!}{2^{4l+1}(l-1)!l!l!(l+1)!}
\tag{24}
$$

Second, it is convenient to rewrite the third term in eq 2 through the coefficients $f_{lm}(\mathbf{r})$ according to

$$
\begin{aligned}
&l_p^2 d \int\int\int \mathrm{d}\mathbf{r}\, \mathrm{d}\mathbf{n}\, \mathrm{d}\mathbf{n}'\, \rho(\mathbf{n},\mathbf{r})\rho(\mathbf{n}',\mathbf{r}) \sin\gamma_{\mathbf{nn}'} \\
&= l_p^2 d \int \mathrm{d}\mathbf{r} \sum_{l=0}^{\infty} \sum_{m=-2l}^{2l} \frac{4\pi d_{2l}}{4l+1} \sum_{l_1,m_1} \sum_{l_2,m_2} f_{l_1m_1}(\mathbf{r}) f_{l_2m_2}(\mathbf{r}) \times \\
&\qquad \int \mathrm{d}\mathbf{n}\, Y_{l_1m_1}(\mathbf{n}) Y_{2lm}(\mathbf{n}) \int \mathrm{d}\mathbf{n}'\, Y_{l_2m_2}(\mathbf{n}') Y^*_{2lm}(\mathbf{n}') \\
&= l_p^2 d \int \mathrm{d}\mathbf{r} \sum_{l=0}^{\infty} \sum_{m=-2l}^{2l} (-1)^m \frac{4\pi d_{2l}}{4l+1} f_{2lm}(\mathbf{r}) f_{2l-m}(\mathbf{r}) \\
&= l_p^2 d \int \mathrm{d}\mathbf{r} \sum_{l=0}^{\infty} \sum_{m=-2l}^{2l} \frac{4\pi d_{2l}}{4l+1} [f_{2lm}(\mathbf{r})]^2
\end{aligned}
\tag{25}
$$

The coefficients $f_{lm}(\mathbf{r})$ can be easily expressed through $q_{lm}(\mathbf{r})$ by expanding both sides of eq 1 into the series of spherical harmonics according to

$$
\begin{aligned}
\rho(\mathbf{n},\mathbf{r}) &= \sum_{l'm'} f_{l'm'}(\mathbf{r}) Y_{l'm'}(\mathbf{n}) \\
&= \psi(-\mathbf{n},\mathbf{r})\psi(\mathbf{n},\mathbf{r}) \\
&= \sum_{l_1,m_1} \sum_{l_2,m_2} (-1)^{l_1} q_{l_1m_1}(\mathbf{r}) q_{l_2m_2}(\mathbf{r}) Y_{l_1m_1}(\mathbf{n}) Y_{l_2m_2}(\mathbf{n})
\end{aligned}
\tag{26}
$$

Multiplication of both sides of eq 26 by $Y^*_{lm}(\mathbf{n})$, integration over $\mathbf{n}$ according to

$$
\begin{aligned}
&\sum_{l',m'} f_{l'm'}(\mathbf{r}) \int \mathrm{d}\mathbf{n}\, Y_{l'm'}(\mathbf{n}) Y^*_{lm}(\mathbf{n}) = \\
&\qquad \sum_{l_1,m_1} \sum_{l_2,m_2} (-1)^{l_1} q_{l_1m_1}(\mathbf{r}) q_{l_2m_2}(\mathbf{r}) \int \mathrm{d}\mathbf{n}\, Y_{l_1m_1}(\mathbf{n}) Y_{l_2m_2}(\mathbf{n}) Y^*_{lm}(\mathbf{n})
\end{aligned}
\tag{27}
$$

and then the use of the normalization condition given by eq 5 for spherical harmonics give eq 10.

The fourth term in eq 7 represents the condition of constant amount of monomer units in the sphere can be derived according to

$$
\begin{aligned}
&\int\int \mathrm{d}\mathbf{n}\, \mathrm{d}\mathbf{r}\, \rho(\mathbf{n},\mathbf{r}) = \int\int \mathrm{d}\mathbf{n}\, \mathrm{d}\mathbf{r}\, \psi(-\mathbf{n},\mathbf{r})\psi(\mathbf{n},\mathbf{r}) \\
&= \int\int \mathrm{d}\mathbf{n}\, \mathrm{d}\mathbf{r} \left[\sum_{l_1,m_1} (-1)^{l_1} q_{l_1m_1}(\mathbf{r}) Y_{l_1m_1}(\mathbf{n}) \right] \left[\sum_{l,m} q_{lm}(\mathbf{r}) Y_{lm}(\mathbf{n}) \right] \\
&= \int \mathrm{d}\mathbf{r} \left[\sum_{l_1,m_1} \sum_{l,m} (-1)^{l_1+m} q_{l_1m_1}(\mathbf{r}) q_{lm}(\mathbf{r}) \right] \int \mathrm{d}\mathbf{n} Y_{l_1m_1}(\mathbf{n}) Y^*_{l-m}(\mathbf{n}) \\
&= \int \mathrm{d}\mathbf{r} \sum_{l,m} (-1)^{l+m} q_{lm}(\mathbf{r}) q_{l-m}(\mathbf{r}) \\
&= \int \mathrm{d}\mathbf{r} \sum_{l,m} (-1)^{l} [q_{lm}(\mathbf{r})]^2 \\
&= \frac{L}{l_p}
\end{aligned}
\tag{28}
$$

Finally, the fifth term in eq 7 specifying the condition of impenetrability of the spherical surface for the polymer can be derived according to

$$
\begin{aligned}
&\int \mathrm{d}\mathbf{n}\mathrm{d}\mathbf{r}\, \rho(\mathbf{n},\mathbf{r})\Big|_{r=R} \\
&= \int \mathrm{d}\mathbf{n}\, \psi(-\mathbf{n},\mathbf{r})\Big|_{r=R} \psi(-\mathbf{n},\mathbf{r})\Big|_{r=R} \\
&= R^2 \iint \mathrm{d}\Theta \mathrm{d}\Phi \sin\Theta \times \\
&\left[\sum_{l_1,m_1} \sum_{l,m} (-1)^{l_1+m} q_{l_1m_1}(R,\Theta,\Phi) q_{lm}(R,\Theta,\Phi) \right] \\
&\qquad \times \int \mathrm{d}\mathbf{n}\, Y_{l_1m_1}(\mathbf{n}) Y^*_{l-m}(\mathbf{n}) \\
&= R^2 \iint \mathrm{d}\Theta \mathrm{d}\Phi \sin\Theta \times \\
&\sum_{l,m} (-1)^{l+m} q_{lm}(R,\Theta,\Phi) q_{l-m}(R,\Theta,\Phi) \\
&= R^2 \iint \mathrm{d}\Theta \mathrm{d}\Phi \sin\Theta \sum_{l,m} (-1)^{l} [q(R,\Theta,\Phi)]^2
\end{aligned}
\tag{29}
$$

Appendix C: Numerical Considerations

In practice, the calculation of density and order parameter profiles using the expansions described in the main text requires truncation of the function expansions given in eqs 3 and 11. The influence of the truncation of the expansion of the segment orientation into spherical harmonics was estimated by considering the reduced system composed of semiflexible polymers in an infinite and homogeneous space.[40,41] For this system, the nematic transition order parameter has been calculated to $S = 0.49$ using an approximative Onsager trial function method,[40] and more accurately[41] $S = 0.46$ using the spherical harmonics expansion method with large number of terms in the expansion. We found that truncation of the sum over l in eq 3 to $l_{\max} = 4$ provided a numerical solution deviating less than 5% from the more accurate solution.[41] Thus, finding that $l_{\max} = 4$ provides a good accuracy for the infinite-space system, we assumed that it would also be a good approximation for our confined system as well.

The influence of the truncation of the segment density expansion according to eq 11 was estimated by examining how (i) the free energy and (ii) the segment density function depended on $i_{\max}$ and $j_{\max}$. We found that already at $i_{\max} = 2$ and $j_{\max} = 1$, a further increase in $i_{\max}$ and $j_{\max}$ affected the free energy less than 10% and only moderately the segment density distribution. Since $\rho \sim q^2$, a truncation to $i_{\max} = 2$ in eq 11 approximates the segment density distribution by a 4th-order polynomial. While using the expansion (11), one has to apply additional physical constraints for the density function $\varphi(\mathbf{r})$ reflecting the fact that the polymer density is homogeneous with respect to r and Θ in the center of the sphere:

$$
\frac{\partial\varphi(0,\Theta)}{\partial r} = \frac{\partial\varphi(0,\Theta)}{\partial\Theta} = 0
$$

In total, we end up with 34 nontrivial expansion coefficients C_{lmij} to be determined by minimization of the variational free energy. We believe that our ansatz provides a general picture of the density and density order; however, we cannot rule out that details are affected by the truncation of the variational ansatz.

References and Notes

(1) Rubinstein, M.; Colby, R. H. *Polymer Physics*; Oxford University Press: New York, 2003.

(2) Alberts, B.; Johnson, A., Lewis, J.; Raff, M.; Roberts, K.; Walter, P. *Molecular Biology of the Cell*, 4th ed.; Garland Science: New York, 2002.
(3) Evilevitch, A.; Castelnovo, M.; Knobler, C. M.; Gelbart, W. M. *J. Phys. Chem B* **2004**, *108*, 6838.
(4) Comolli, L. R.; Spakowitz, A. J.; Siegerist, C. E.; Jardine, P. J.; Grimes, S.; Anderson, D. L.; Bustamante, C.; Downing, K. H. *Virology* **2008**, *371*, 267.
(5) Cerritelli, M. E.; Cheng, N.; Rosenberg, A. H.; McPherson, C. E.; Booy, F. P.; Steven, A. C. *Cell* **1997**, *91*, 271.
(6) Zhang, Z.; Greene, B.; Thuman-Commike, P. A.; Jakana, J.; Prevelige Jr, P. E.; King, J.; Chiu, W. *J. Mol. Biol.* **2000**, *297*, 615.
(7) Olson, N. H.; Gingery, M.; Eiserling, F. A.; Baker, T. S. *Virology* **2001**, *279*, 385.
(8) Leforestier, A.; Livolant, P. *J. Mol. Biol.* **2010**, *396*, 384.
(9) Petrov, A. S.; Harvey, S. C. *Structure* **2007**, *15*, 21.
(10) Hu, T.; Shklovskii, B. I. *Phys. Rev. E* **2007**, *75*, 051901.
(11) Van der Schoot, P.; Bruinsma, R. *Phys. Rev. E* **2005**, *71*, 061928.
(12) Rudnick, J.; Bruinsma, R. *Phys. Rev. Lett.* **2005**, *94*, 038101.
(13) Kindt, J.; Tzlil, S.; Ben-Shaul, A.; Gelbart, W. M. *Proc. Natl. Acad. Sci. U.S.A.* **2001**, *98*, 13671.
(14) Tzlil, S.; Kindt, J. T.; Gelbart, W. M.; Ben-Shaul, A. *Biophys. J.* **2003**, *84*, 1616.
(15) Purohit, P. K.; Kondev, J.; Phillips, R. *Proc. Natl. Acad. Sci. U.S.A.* **2003**, *100*, 3173.
(16) LaMarque, J. C.; Le, T. L.; Harvey, S. C. *Biopolymers* **2004**, *73*, 348.
(17) Metzler, R.; Dommersnes, P. G. *Eur. Biophys. J.* **2004**, *33*, 497.
(18) Cerda, J. J.; Sintes, T.; Chakrabarti, A. *Macromolecules* **2005**, *38*, 1469.
(19) Angelescu, D. G.; Bruinsma, R.; Linse, P. *Phys. Rev. E* **2006**, *73*, 041921.
(20) Angelescu, D. G.; Linse, P.; Nguyen, T. T.; Bruinsma, R. F. *Eur. Phys. J. E* **2008**, *25*, 323.
(21) Katzav, E.; Adda-Bedia, M.; Boudaoud, A. *Proc. Natl. Acad. Sci. U.S.A.* **2006**, *103*, 18900.
(22) Boue, L.; Katzav, E. *Europhys. Lett.* **2007**, *80*, 54002.
(23) Klug, W. S.; Ortiz, M. *J. Mech. Phys. Sol.* **2003**, *51*, 1815.
(24) Klug, W. S.; Feldman, M. T.; Ortiz, M. *Comput. Mech.* **2005**, *35*, 146.
(25) Li, Z.; Wu, J.; Wang, Z.-G. *Biophys. J.* **2008**, *94*, 737.
(26) Odijk, T. *Biophys. J.* **1998**, *75*, 1223.
(27) Siber, A.; Dragar, M.; Parsegian, V. A.; Podgornik, R. *Eur. Phys. J. E* **2008**, *26*, 317.
(28) Spakowitz, A. J.; Wang, Z.-G. *Biophys. J.* **2005**, *88*, 3912.
(29) Spakowitz, A. J.; Wang, Z.-G. *Phys. Rev. Lett.* **2003**, *91*, 166102.
(30) Marenduzzo, D. *Europhys. Lett.* **2009**, *85*, 38005.
(31) Hud, N. V. *Biophys. J.* **1995**, *59*, 1355.
(32) Forrey, C.; Muthukumar, M. *Biophys. J.* **2006**, *91*, 25.
(33) Angelescu, D. G.; Linse, P. *Phys. Rev. E* **2007**, *75*, 051905.
(34) Angelescu, D. G.; Stenhammar, J.; Linse, P. *J. Phys. Chem. B* **2007**, *111*, 8477.
(35) Angelescu, D. G.; Linse, P. *Soft Matter* **2008**, *4*, 1981.
(36) Angelescu, D. G.; Linse, P. *Curr. Opin. Colloid Interface Sci.* **2008**, *13*, 389.
(37) Arsuaga, J.; Tan, R. K.-Z.; Vazquez, M.; Sumnersa, D. W.; Harvey, S. C. *Biophys. Chem.* **2002**, *101*, 475.
(38) Nguyen, T. T.; Bruinsma, R. F.; Gelbart, W. M. *Phys. Rev. Lett.* **2006**, *96*, 078102.
(39) Onsager, L. *Ann. N.Y. Acad. Sci.* **1949**, *51*, 627.
(40) Khokhlov, A. R.; Semenov, A. N. *Physica A* **1981**, *108*, 546.
(41) Vroege, G. J.; Odijk, T. *Macromolecules* **1988**, *21*, 2848.
(42) Landau, L. D.; Lifshitz, E. M. *Theory of Elasticity*; Pergamon Press: New York, 1970.
(43) de Gennes, P. G.; Prost, J. *The Physics of Liquid Crystals*, 2nd ed.; Clarendon Press: Oxford, UK, 1993.
(44) Grosberg, A. Yu.; Pachomov, D. V. *Liq. Cryst.* **1991**, *10*, 539.
(45) Grosberg, A. Yu.; Khokhlov, A. R. *Statistical Physics of Macromolecules*; AIP Press: New York, 1994.
(46) Cui, S.-M.; Akcakir, O.; Chen, Z. Y. *Phys. Rev. E* **1995**, *51*, 4548.
(47) Chen, Z. Y.; Cui, S.-M. *Phys. Rev. E* **1995**, *52*, 3876.
(48) Arfken, G. *Mathematical Methods for Physicists*, 3rd ed.; Academic Press: Orlando, FL, 1985.
(49) Holyst, R.; Oswald, P. *Macromol. Theory Simul.* **2001**, *10*, 1.
(50) Fournier, J.-B.; Galatola, P. *Europhys. Lett.* **2005**, *72*, 403.
(51) Purohit, P. K.; Inamdar, M. M.; Grayson, P. D.; Squires, T. M.; Kondev, J.; Phillips, R. *Biophys. J.* **2005**, *88*, 851.
(52) Cifra, P.; Bleha, T. *Eur. Phys. J. E* **2010**, *032*, 273.
(53) Lander, G. C.; Tang, L.; Casjens, S. R.; Gilcrease, E. B.; Prevelige, P.; Poliakov, A.; Potter, C. S.; Carragher, B.; Johnson, J. E. *Science* **2006**, *312*, 1791.
(54) Semenov, A. N.; Khokhlov, A. R. *Vysokomolek. Soed. (Polym. Sci. USSR)* **1982**, *24A*, 2573.
(55) Potemkin, I. I.; Limberger, R. E.; Kudlay, A. N.; Khokhlov, A. R. *Phys. Rev. E* **2002**, *66*, 011802.
(56) Potemkin, I. I.; Oskolkov, N. N.; Khokhlov, A. R.; Reineker, P. *Phys. Rev. E* **2005**, *72*, 021804.

JP108461Z